Systematic approach for determination of equilibrium atomic surface structure

John C. Thomas,[1] Normand A. Modine,[2] Joanna Mirecki Millunchick,[1] and Anton Van der Ven[1,*]
[1]*Department of Materials Science and Engineering, University of Michigan, Ann Arbor, Michigan 48109, USA*
[2]*Center for Integrated Nanotechnologies, Sandia National Laboratories, Albuquerque, New Mexico 87185, USA*
(Received 23 July 2010; published 20 October 2010)

Despite the increasing importance of atomic-scale surface characterization, the state of the art in automating the prediction of atomic surface structure lags behind recent advances in bulk structure prediction. In this paper we present an approach whereby poorly characterized equilibrium surface structure can be systematically determined via a two-step process and apply this approach to the GaAs(001) surface. First we demonstrate that trends in complex surface structure are reducible to a small set of basic structural rules which can then be used to efficiently generate many likely surface reconstruction prototypes. Second we use first-principles energy calculations to screen for low-energy prototypes and apply the cluster expansion formalism to explore the effect of configurational excitations at surface sites capable of low-energy species substitution. Using this method, we generate a database of all likely reconstruction prototypes for the group-V-rich III-V (001) surface, which is then used to obtain the GaAs(001) reconstruction phase diagram from first principles. We also identify a class of (4×3) reconstructions that is nearly stable on pure GaAs and is likely important in kinetically limited growth regimes and on strain-stabilized III-V alloy surfaces.

DOI: 10.1103/PhysRevB.82.165434 PACS number(s): 68.35.B−, 68.35.Md, 68.47.Fg

I. INTRODUCTION

At the surface termination of most covalently bonded solids, atoms relax to configurations different from those observed in the bulk material. These relaxations are driven by the strong chemical, elastic, and electrostatic interactions between atoms that arise from highly directional orbitals and the broken symmetry imposed at surfaces. The resulting thermodynamically stable structure, or surface reconstruction, is uniquely determined by the experimentally accessible thermodynamic parameters present at the surface and plays an important role in determining surface and interfacial properties. Surface reconstructions are known to affect epitaxial growth,[1] catalysis,[2] oxide formation,[3] and magnetic domain ordering,[4] making them of considerable interest for a range of applications. Unfortunately, full characterization of the atomic-scale structural details of surface reconstructions has proven difficult for some systems. Although reconstruction periodicity and symmetry can usually be inferred experimentally via diffraction and microscopy techniques, a number of experimentally observed reconstructions still lack proven structural models. Examples include the $(1\times5)/c(2\times10)$ reconstruction on GaSb(001) (Ref. 5) and a number of interesting oxygen adsorbate structures on Ag(111).[6]

In alloy systems, where two or more of the constituent species may be chemically similar, surface reconstructions are significantly more difficult to characterize since configurational order of the alloy species plays an important role in determining stability. A notable example is the alloying of chemically similar Ga and In on the $In_xGa_{1-x}As$ (001) ternary surface, where the (4×3) and (6×4) reconstructions are observed.[7] Where poorly characterized surfaces exist, these gaps in understanding hinder the development of comprehensive thermodynamic and kinetic models of important phenomena (e.g., epitaxial growth, morphological evolution, heterointerface abruptness, alloy segregation, and surface diffusion).

Significant progress has been made in recent decades to uncover structural details of surface reconstructions from experiment and theory, but the typical process is an arduous one that, at its root, is physically guided by trial and error. Although powerful real-space and reciprocal-space experimental characterization techniques are available, it is sometimes difficult to determine more information than the surface unit cell lattice vectors and general compositional trends. Theoretical study of thermodynamic stability is largely based on high-accuracy total energy calculations performed using density-functional theory (DFT). Although DFT can be used to study very small differences in structure, such calculations are computationally intensive, and without a physically informed way to narrow the search for structural models, a search for equilibrium surface structure can become intractable.

While a number of promising approaches have been implemented to predict bulk crystal structure theoretically, prominent among them being genetic programming strategies[8] or data mining of materials databases,[9,10] far less progress has been made to formalize the prediction of surface structure. Genetic structural optimization techniques have been used to determine equilibrium surface structure in single-component systems,[11] but since genetic optimization typically requires many hundreds or thousands of energy calculations, it is ill-suited for multicomponent surfaces, or when first principles accuracy is desired. Data mining approaches, on the other hand, are difficult to envision for surface systems since the set of likely surface reconstructions of a material depends largely on the bulk crystal of the substrate and the surface of interest. Because these preliminary conditions are so varied, many of the more intriguing surface characterization problems likely arise from previously unencountered reconstructions, a situation that limits the usefulness of a data-mining approach.

In some instances the degrees of freedom that dominate surface reconstruction can be mapped onto a two-dimensional (2D) lattice model. The cluster-expansion tech-

nique can then be employed to efficiently search for thermodynamically stable reconstructions.[12,13] This approach has been used to study a simple model of As adsorption and surface alloying in InAs/GaAs(001).[14] Unfortunately, because it is an on-lattice model, the cluster expansion in its typical form is ill-suited to describe the more complicated structural degrees of freedom or symmetry-breaking local relaxations that may occur at the surface of many technologically important solids.

The need for a more systematic approach to determining equilibrium surface structure has been motivated by our particular interest in the zincblende III-V (001) surface, which has a number of poorly understood surface reconstructions, both in the pure compounds and in their alloys. Even in the GaAs(001) system, which is relatively well characterized, there are longstanding experimental observations of surface symmetries that have yet to be adequately explained by accurate structural models. In 1989 Däweritz and Hey[15] determined a reconstruction phase diagram from reciprocal space measurements of the GaAs(001) surface that includes (2×3) and (1×3) periodicities at low temperature, and (4×6) and (3×6) periodicities at Ga-rich conditions, none of which can be explained within the current theoretical understanding of the system.

Our current work is focused on the $(n\times3)$ and $c(6\times4)$ reconstructions,[7,16] both observed over a range of x on $In_xGa_{1-x}As$ (001). In particular, we hope to determine the atomic structure of the $(n\times3)$ reconstruction and the mechanism that allows it to coexist as nanoscale domains with other reconstructions. The nanoscale coexistence of the $(n\times3)$ is especially puzzling since the small domain size is in contrast to the traditional picture of coexistence in which domains tend to maximize their size at equilibrium in order to minimize boundary energies. Additionally, the presence of a coexistence is in apparent contradiction to the Gibbs phase rule, which allows phase coexistence only when an extensive parameter of the system is fixed. This suggests that the coexistence must be strain stabilized via interaction with the substrate,[17] meaning that the range of parameters over which the $(n\times3)$ is stable as a pure phase may be very small, if they are experimentally accessible at all. The necessary first step in resolving the $(n\times3)$ stability problem is to identify likely structural candidates for this reconstruction by first generating a database of structurally promising candidates and then screening them based on both physically derived heuristics and first-principles energy calculations on pure InAs or GaAs.

Here we present a systematic approach for determining equilibrium atomic surface structure in III-V compound semiconductors. The approach is described in two steps due to the nature of multicomponent surface reconstructions; a fully defined reconstruction consists of a *reconstruction prototype* (i.e., the pattern of bonds that describe the topology of the reconstruction) and the *species configuration* (i.e., the distinct arrangement of atomic species on the sites of the reconstruction prototype). Accordingly, the two steps are as follows: (i) explore structural degrees of freedom to generate candidate reconstruction prototypes and use first-principles methods to identify low-energy prototypes. (ii) Use the cluster expansion formalism[12] to describe the energetics of species configuration for low-energy prototypes in order to identify the thermodynamically stable reconstructions, each consisting of a reconstruction prototype plus a species configuration of that prototype.

For the first step we introduce an algorithm to generate structurally plausible reconstruction prototypes based on observed or proposed structural motifs. A distinguishing feature of III-V (001) surfaces is the in-plane bonding between neighboring atoms giving rise to the "surface dimer" and "backbond" motifs. In compound materials, some sites of a surface reconstruction prototype may be able to host more than one species of atom. In III-V systems this is most readily observed by the formation of *heterodimers*, where a terminating dimer consists of one cation species and one anion species. The possibility of multiple distinct heterodimer arrangements necessitates the second step of our approach in which we use density-functional theory energy calculations to determine the energetic role of these configurational degrees of freedom. The cluster-expansion method from alloy theory[12,13] is then applied to these data to predict energies across the entire configuration space of a single reconstruction prototype, making Monte Carlo methods accessible as a means to conduct comprehensive thermodynamic analysis at finite temperature.

We apply this method to the (001) surface of the zincblende III-V compounds with the ultimate goal of identifying the energetically competitive reconstructions of this surface that either are stable for a pure binary compound or are likely to become stable upon perturbing the binary system (e.g., by introducing strain or alloying). Several specific surface reconstructions of the III-V binary compounds have been well characterized, allowing us to develop a set of structural rules that recreate these and similar reconstruction prototypes, while excluding prototypes with unobserved and nonphysical features. An implementation of our enumeration algorithm incorporating these structural rules is used to generate all likely surface reconstructions of a given unit cell area. We present a statistical characterization of the generated reconstruction prototypes and examine their excess charge characteristics, which are determined by an efficient formulation of the electron-counting method (ECM).[18] The database of generated reconstructions provides a valuable tool for identifying the structure of poorly characterized binary and alloyed III-V semiconductor surfaces.

We examine reconstruction stability by calculating surface free energies from first principles for all charge-neutral reconstruction candidates having experimentally observed surface lattice vectors on GaAs(001). These results verify the accepted GaAs(001) phase diagram and reveal near-stable reconstructions, including a class of (4×3) surface reconstructions that is nearly stable for GaAs(001). Variants of this $h0(4\times3)$ prototype may occur as a kinetically trapped reconstruction at low temperature or could potentially be stabilized by alloying effects in the ternary $In_xGa_{1-x}As$. Finite temperature Monte Carlo free energies are compared for this reconstruction prototype and the well-known GaAs $c(4\times4)$ in order to determine relative stability in a way that accounts for the entropic contribution of species configuration.

II. METHODOLOGY

A. Structural trends of III-V structures

The bulk zincblende crystal of III-V compounds is comprised of two sublattices, in which each atom of one sublattice shares four tetrahedrally oriented bonds with atoms of the other sublattice. Along the [001] direction, the crystal exhibits an ABCD stacking of square 2D lattices, with A and C layers belonging to the Group V, or anion, sublattice and B and D layers belonging to the Group III, or cation, sublattice. The stability of zincblende phases of many III-V compounds is due to the sp^3 hybridization of the constituent atomic orbitals, as well as the strong energetic preference for III-V bonds over V-V or III-III bonds. Although the surface is necessarily less well behaved than the bulk, careful consideration of the various III-V reconstruction models that have been predicted to be low in energy from first principles reveals a number of consistent structural traits that nearly all of them share.

We focus here on the class of III-V reconstructions that are group V rich. Bonding orbitals at these surfaces are predominantly sp^3 in character since full filling of $\sigma(sp^3)$ bonding orbitals can be realized by group V-group V and group III-group V bonds. This results in predominantly tetrahedral bond angles, leading to surface structural motifs that can be accommodated easily by the substrate.

As illustrated in Fig. 1(a), we can define two directions specific to each sublattice—the "dimer" axis and the "nondimer" axis. The dimer axis is normal to the plane spanned by the two bulk-oriented tetrahedral bonds while the nondimer axis is perpendicular to the dimer axis in the (001) plane. These axes and the [001] axis are mutually orthogonal, and all atoms of one sublattice share the same dimer and nondimer axes. Thus, in terms of the directions defined in Fig. 1(a) for GaAs, [110] is the dimer axis of the Ga sublattice and the nondimer axis of the As sublattice, while $[1\bar{1}0]$ is the dimer axis of the As sublattice and the nondimer axis of the Ga sublattice.

We have ordered the observed III-V structural traits in a hierarchy, beginning with the least likely to be violated: (1) *all atoms have threefold or fourfold coordination.* This requirement is necessary for each anion to have either sp^3-like bonding, or p^3-like bonding with a filled s-like orbital, and for each cation to have either sp^3-like bonding, or sp^2-like bonding with an empty p-like orbital. Threefold coordinated anions typically have a filled valence orbital which does not participate in bonding, referred to as a "dangling bond."

(2) *There are no vacancies below surface layers.* The presence of a vacancy would significantly distort surrounding bonds and likely lead to high-energy strain and electrostatic interactions. This observation implies that any atom of the structure must sit above and between two other atoms, along the dimer axis of the two lower atoms.

(3) *Anions and cations form dimers along the dimer axis.* If no atom sits in the layer above two atoms that are in-plane neighbors along their dimer axis, these two atoms may bond to form a dimer. Dimers reduce the number of high-energy dangling bonds at the expense of introducing some degree of strain due to the relaxation of the dimerized atoms toward each other. The prototypical III-V anion dimer is illustrated in detail in Fig. 1(a). Dimerization is essentially a way to increase the coordination of atoms via local relaxations. This, along with the first two rules, implies that every atom must have at least one neighbor along the dimer axis in the same (001) plane. Figure 1(b) shows dimerization in the anion

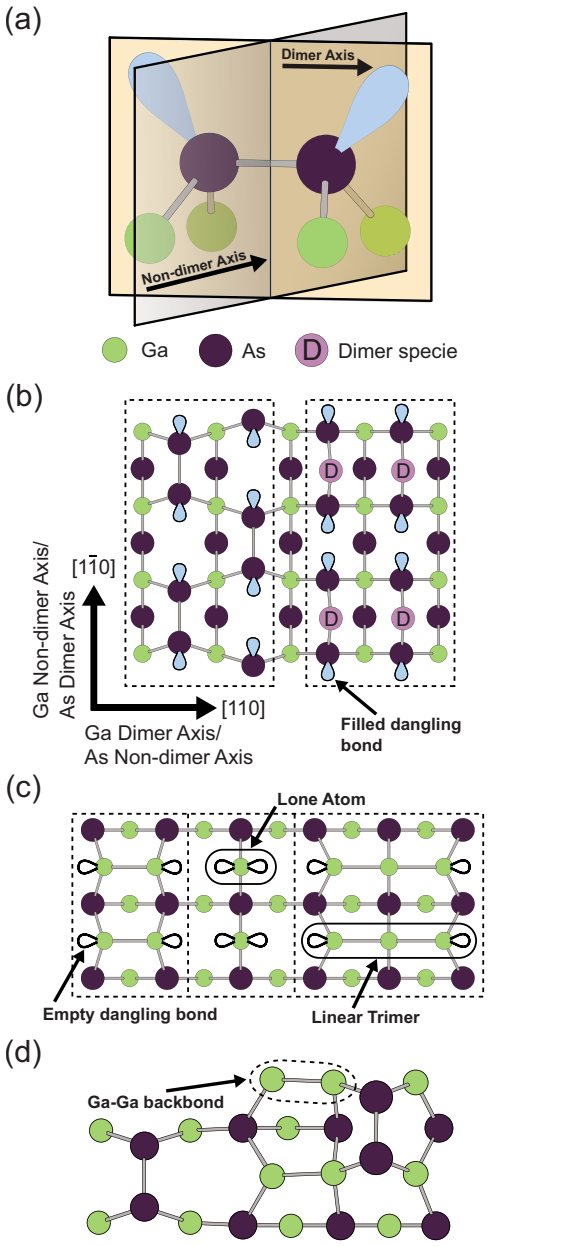

FIG. 1. (Color online) III-V (001) surface structure trends shown for GaAs. (a) As dimer, in perspective, with filled dangling bonds. The nondimer axis is normal to the plane spanned by the dimer and dangling bond. (b) The As-terminated (001) surface with two possible dimerizations. Dimers on the left are depicted in the usual manner; dimers on the right are depicted using the dimer "specie" abstraction. (c) The Ga-terminated (001) surface, with three different bonding motifs: surface dimers, with two three-fold coordinated atoms; lone atoms, with two dangling bonds each; and linear trimers, with a central four-fold coordinated atom. (d) The $\alpha 2(2\times 4)$ reconstruction with Ga-Ga backbond indicated by a dashed oval. [(b)–(d)] Share the same crystal axes.

layer and Fig. 1(c) shows dimerization in the cation layer.

(4) *Backbonds may form between a lone atom and a neighboring threefold coordinated atom.* Backbonds are the second type of in-plane bonding. Unlike dimers, a backbond joins a threefold coordinated atom to a fourfold coordinated atom in the same (001) plane along the plane's dimer axis. Because relaxation of the fourfold coordinated atom is limited, the local relaxation associated with backbonds often results in more highly strained motifs than are caused by the dimer in-plane bond. A group III-group III backbond is a prominent feature of the $\alpha 2(2\times 4)$ reconstruction, which is shown in Fig. 1(d) (backbond is circled).

(5) *A fourfold coordinated atom may not have an in-plane bond, unless it is a backbond.* This rule prevents situations where two threefold coordinated neighboring atoms form an in-plane bond with each other, essentially "bridging the trench." It also prevents the formation of linear trimers, tetramers, and so on. As noted for dimers or backbonds, neighboring atoms must locally relax in order to obtain a separation near the equilibrium in-plane bond length. Such relaxation is significantly more difficult to achieve in bridged or linear polymer motifs. Consequently, these motifs are largely unphysical from an energetic standpoint. Although a linear tetramer structure has been proposed for the GaN(001) (4×1) surface,[19] later work has cast doubt on this model.[20] The illustration in Fig. 1(c) compares motifs with different numbers of in-plane bonds, including a linear trimer.

The formation of dimers and backbonds at the III-V (001) surface inevitably leads to threefold coordinated atoms, implying that some sp^3-hybridized orbitals do not participate in bonding. These so-called dangling bonds cannot be completely filled with electrons while simultaneously maintaining the local charge neutrality of the crystal. As a result, the dangling bonds must be either partially or selectively filled. Energy levels of the hybridized orbitals have been estimated from energies of the s and p orbitals, and compared to the conduction-band maximum and valence-band minimum energies of the bulk crystal.[21] For most III-V materials, the cation dangling bond states are estimated to lie in the conduction band, and are therefore empty, while the anion dangling bond states are estimated to lie in the valence band, and thus are filled. Based on these estimates, a heuristic rule was formulated in the form of the ECM,[18] which demands that the number of electrons required to fill all bonding orbitals and anion dangling bonds is exactly equal to the number of valence-shell electrons donated by the constituent atoms. Experimental and theoretical evidence for the ECM heuristic is prevalent and we have encountered little compelling theoretical evidence in the literature for violations of ECM in polar III-V materials at equilibrium. There is also limited experimental evidence of ECM violation with the extremely Sb-rich $c(2\times 10)$ reconstruction on GaSb (001) (Ref. 22) and the Bi-stabilized (2×1) reconstruction observed on the (001) surface of GaAs and InP (Ref. 23) being notable cases. The ECM is also applicable to a number of other chemistries important to semiconductors and it is the heuristic we use as a first-pass screen to determine thermodynamic stability.

If we take the first three structural rules enumerated above as given, we can construct an expression for the electron-counting rule that is general for all candidate structures generated by our algorithm (as well as those with "bridged" motifs, which we have excluded). As is shown in Appendix A, the net contribution to the excess charge arising from bilayer j can be written

$$(\Delta q)_j = 3(N_{i+1} - N_i) + 2(D_i - D_{i+1}), \tag{1}$$

where N_i denotes the number of atoms and D_i denotes the number of in-plane bonds (i.e., dimers or backbonds) in layer i. Atomic layers i and $i+1$ comprise bilayer j, where i and j increase in the direction away from the substrate. An additional charge of $\frac{3}{2}N_A$ is contributed from the cation-terminated substrate, where N_A is the integral unit area of the unit cell (essentially, the number of atoms in a full monolayer). First-principles calculations bear out the presumed energy penalty imposed by excess surface charge and thus charge neutrality as predicted by the ECM should be considered as an additional structural criterion. Accordingly, we focus on charge-neutral structures in this work although the screening is performed as a final step of prototype generation so that generality is preserved.

B. Algorithm to generate surface reconstruction prototypes

The above rules are incorporated in an algorithm to enumerate III-V reconstruction prototypes. The specific form of the algorithm presented here is based on knowledge of the III-V (001) system (e.g., the bulk crystal and the structural rules we have outlined), although it can be easily adapted to study a range of other systems, provided that basic structural information is known. Surface atoms are assumed to reside at well-defined lattice sites, to within bond-preserving local relaxations. For anion-rich III-V surfaces these sites are assumed to coincide with the bulk zinc-blende lattice positions although additional interstitial sites may be necessary to describe other systems. The algorithm takes as input the surface lattice vectors of the desired unit cell.

The surface unit cell has an associated integral unit area, N_A, which is the number of atoms in a complete bulklike monolayer of the specified unit cell. Because the 1×1 surface lattice vectors lie along the face diagonals of the zinc-blende cubic unit cell, the surface lattice parameter is given by $a_{surf} \equiv a_{bulk}/\sqrt{(2)}$ so that the unreconstructed surface has one atom per unit area a_{surf}^2. In general, a unit cell with lattice vectors $\mathbf{v}=(v_{[110]}, v_{[1\bar{1}0]})$ and $\mathbf{w}=(w_{[110]}, w_{[1\bar{1}0]})$ in terms of the [110] and $[1\bar{1}0]$ unit vectors has an integral unit area

$$N_A \equiv \det\begin{pmatrix} v_{[110]} & v_{[1\bar{1}0]} \\ w_{[110]} & w_{[1\bar{1}0]} \end{pmatrix} / a_{surf}^2. \tag{2}$$

Of the large superset of structures that could be obtained via a brute-force enumeration, many are symmetrically equivalent or are structurally incompliant (i.e., they do not obey our structural rules). The goal of the algorithm is to find the subset of reconstruction prototypes that are both structurally compliant and symmetrically distinct while limiting the total number of structures that must be evaluated. This is done efficiently by constructing the reconstruction prototypes layer-by-layer, from the substrate up, screening at each

layer for structural compliance and symmetrical uniqueness. Consider the $n=0$ atomic layer, which represents the first layer of substrate, sitting at the surface of a semi-infinite bulk crystal. Atop this layer, the $n=1$ layer is placed, which consists of some arrangement of atoms and vacancies on the N monolayer sites of the unit cell that coincide with the ideal bulk lattice positions. All 2^N possible layer configurations are considered, keeping only one instance of each symmetrically distinct monolayer configuration and subsequently excluding all configurations that are not allowed in a structurally compliant prototype. On top of each compliant $n=1$ layer configuration we specify a 2D crystal for the $n=2$ layer that is selected from ideal bulk lattice positions such that each site has two nearest neighbors in the $n=1$ layer, per the second structural rule. Structurally compliant configurations of atoms and vacancies in the $n=2$ layer are enumerated, and each subsequent layer is constructed in this manner. When the nth layer configuration results in all n layers being structurally compliant, this n-layer structure is a valid reconstruction prototype and is added to the database.

We limit the possibility of constructing fully filled substratelike layers in order to prevent the generation of prototypes that are identical upon c-axis translation (normal to the surface). With this criterion in place there are always more atoms in layer $n-1$ than in layer n so that the construction process will eventually terminate when no new layer can be constructed that obeys the structural rules. For most systems in which there are no bonds normal to the surface plane, which include zinc blende (001), structural rule two is sufficient to ensure self-termination. In other systems, such as the simple cubic (001), additional criteria would have to be specified. The impossibility of c-axis translational symmetry of two generated structures also ensures that if two structures in progress are identical up to layer $n-1$ but differ in layer n, all prototypes spawned from the first structure will be distinct from all prototypes spawned from the second structure.

We abstract the in-plane bond as a distinct structural element, which we refer to as the "dimer specie." This structural abstraction is an essential feature of the algorithm that is necessary to distinguish between distinct arrangements of dimers and backbonds on otherwise identical monolayer configurations of atoms and vacancies, as illustrated in Fig. 5(b). In the implementation of the algorithm the dimer specie is treated identically to an atomic species for the purpose of identifying symmetries and enumerating monolayer configurations. A dimer specie can be placed on a regular lattice site in layer n to indicate that its two nearest neighbor atoms in layer $n-1$ are bonded in-plane along the $n-1$ layer dimer axis, as shown in Fig. 1(b). The algorithm can be implemented as described previously, except that layers are enumerated as configurations of atoms, vacancies, and dimer species. Additional restrictions prevent atoms or dimer species in layer n having dimer specie nearest neighbors in layer $n-1$ and dimer species within a layer are not allowed to neighbor along the layer's non-dimer axis.

Constructing the candidates layer-by-layer from the substrate simplifies the enumeration problem significantly by restricting the number of relevant configurations at each step. With the inclusion of a dimer specie, there are at most 3^{N_A} configurations for the first layer and significantly fewer for each subsequent layer. The main computational bottleneck is the filtering of equivalent configurations during enumeration, for which we utilized an algorithm similar to that described by Ferreira, Wei and Zunger,[24] whereby a set of configurational basis functions are used to construct a mathematical description of configuration that is invariant under Euclidean transformations. This method is significantly faster than direct geometric comparison, though faster methods exist.[25]

C. Identifying low-energy reconstructions and exploring configurational degrees of freedom

Up to this point, we have discussed the generation of reconstruction prototypes without explicitly specifying the species occupying their lattice sites. In order to ultimately determine the relative stability of the generated structures we must identify the low-energy configurations of atomic species on the prototype lattices. The simplified form of the ECM [Eq. (1)] is derived in the AppendixA under the assumption that the surface is composed of single-species monolayers that alternate between group III and group V, as in the substrate. Species substitution in the bulk, where atoms are fourfold coordinated, is considered an antisite defect. An antisite defect results in a net change of +2 or −2 electrons from the substitution of a cation for anion, or visa versa, without any commensurate change in the number of bonds or valence-band dangling orbitals to accommodate the difference in charge. However, if an atom at a threefold coordinated site is substituted, the dangling bond of that site moves from the conduction band to the valence band, or visa versa, accommodating the difference in charge. Consequently, while the formation energy of antisite defects at fourfold coordinated sites, even near the surface, is quite high, the energy of species substitution at *threefold coordinated sites* is comparatively low. Scanning tunnel microscope (STM) studies of III-V surfaces suggest that configurational fluctuations of the threefold sites of surface dimers, resulting in creation of heterodimers, do occur.[26]

Because of the large difference in substitutional energy between threefold and fourfold coordinated sites, we assume that the configuration of fourfold coordinated sites is fixed to the bulklike configuration. However, there is an additional configurational degree of freedom associated with each threefold coordinated site of a reconstruction prototype. Specifically, there are 2^{N_3} possible configurations of cations and anions on the N_3 threefold coordinated sites contained in the prototype unit cell. Testing all possible configurations of all generated prototypes is a hopelessly intensive and impractical task. Thus, the second step in determining the equilibrium GaAs(001) surface structure focuses on refining the search to a reduced set of reconstruction prototypes and then identifying ground-state configurations of Ga and As on their threefold coordinated surface sites.

We refine the search for a reconstruction ground state (i.e., a reconstruction prototype plus it lowest energy configuration of species at threefold coordinated sites) in two steps. In the first step, we calculate an energy for each prototype, assuming an As-rich surface, and identify the lowest energy prototypes (e.g., those within 50 meV of being

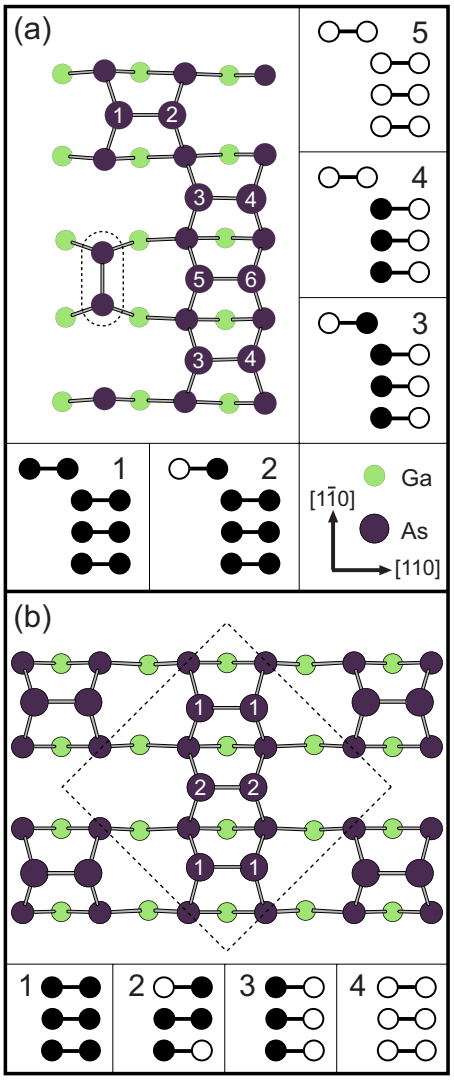

FIG. 2. (Color online) Depiction of dimer sites considered for species substitution in the cluster expansions as well as low-energy configurations of these sites (schematic insets). The sites included in the cluster expansion are indicated by white numbers, where equivalent sites share the same number. Low-energy configurations larger than the unit cell are not depicted. In configuration schematics, black are As, white are Ga. (a) The $h0(4\times3)$ prototype and five low-energy dimer site configurations. (b) The $c(4\times4)$ prototype and four low-energy dimer site configurations.

stable). Once a low-energy reconstruction prototype is identified, we proceed to the second step by collecting the threefold coordinated sites of the prototype and mapping them onto a two-dimensional substitutional lattice model. This lattice contains the sites that have a Ga-As substitutional degree of freedom. Figure 2 shows the lattice of selected substitutional sites for two specific reconstruction prototypes (sites where Ga-As substitution is allowed are indicated by numbers).

Once such a lattice has been defined, the cluster-expansion formalism, which is widely used in alloy theory, can then be used to parameterize the configurational dependence of the surface energy in terms of configurational basis functions. To construct the basis functions we first assign an occupation variable p_i to each threefold coordinated site i, where $p_i=0$ indicates As occupancy and $p_i=1$ indicates Ga occupancy; this choice of allowed occupation values is particularly well-suited for the As-rich regime.[27] Within this description the configuration of the entire N_3-site lattice is specified exactly by the vector $\vec{p}=(p_1,p_2,\ldots,p_i,\ldots,p_{N_3})$. We define a configurational basis function as the product of occupation variables of all sites comprising the cluster α

$$\Gamma_\alpha(\vec{p}) = \prod_{i\in\alpha} p_i. \tag{3}$$

Here α can be a single site, pair, triplet, or other cluster of sites on the lattice. The Γ_α comprise a complete and orthonormal basis set that spans the configurational space associated with the sublattice of threefold coordinated sites.[12,13] Thus, using this basis it is possible to exactly represent the configurational dependence of the surface energy of a reconstruction prototype. Formally, this representation of the energy is the series expansion

$$E(\vec{p}) = \sum_{\{\alpha\}} V_\alpha \Gamma_\alpha(\vec{p}), \tag{4}$$

where the sum is taken over all possible clusters of sites on the lattice. The constant coefficient V_α is the effective cluster interaction (ECI) arising from cluster α.

Although the expression of Eq. (4) is exact, the contribution to the Hamiltonian from clusters consisting of many sites or of sites separated by large distances is often vanishingly small. Additionally, crystal symmetry renders many clusters identical, in which case they have the same ECI. This means that in practice it is only necessary to determine ECI for a small subset of cluster basis functions to accurately predict the surface energy. The ECI may be determined using a sufficiently large dataset of configurational energies calculated from first principles to produce a very accurate predictive model. We select the basis functions to include in the cluster expansion by targeting a minimal value of the leave-one-out cross-validation score.[28] Detailed descriptions of the formalism and methodology for selecting basis functions of surface lattices and determining their ECI can be found in the literature.[14,29,30]

The cluster expansion is a valuable tool for identifying configurational ground states, which can be found either by directly enumerating lattice configurations and evaluating their energy via the cluster expansion or by simulated annealing within Monte Carlo simulation. Monte Carlo can also be used to determine the finite-temperature surface free energy of a reconstruction prototype, which is affected by thermal excitations of configuration. By comparing the free energies of various low-energy reconstruction prototypes, a finite-temperature phase diagram can be determined.

III. RESULTS

A. Statistical analysis

Using the algorithm described above along with our structural rules for III-V surfaces, we have enumerated all reconstruction prototypes of the III-V (001) zinc-blende surface up

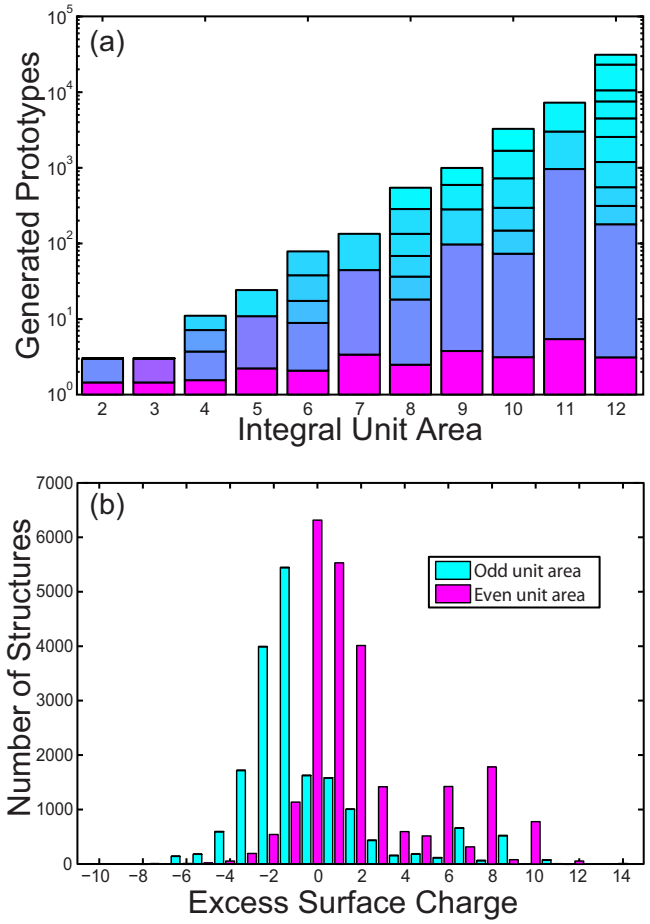

FIG. 3. (Color online) Statistical characterization of the III-V surface reconstructions prototype database generated by the algorithm presented in Sec. II B. (a) Total number of generated structures for each unit cell area, up to $N_A=12$. Bar subdivisions are proportional to the number of generated prototypes for each supercell shape. Topmost sections correspond to square (or near-square) supercells and aspect ratio increases down the bar. Color indicates area-normalized aspect ratio for comparison of supercell shapes with different area. (b) Histogram of excess surface charge incidence for the generated prototype database, as determined by the ECM. Distinction between supercells with odd or even integral unit area is indicated.

to $N_A=12$ [i.e., all supercells containing 12 or fewer (1×1) surface cells] within the Group V-rich regime. Figure 3(a) shows the number of generated structures for each supercell area. The total for each volume is subdivided by supercell shape. Interestingly, the supercell shapes that account for the largest portion of candidate structures (nearly 50%) have aspect ratio much higher than 1 with perpendicular (or nearly perpendicular) lattice vectors. These supercells, which have one lattice vector of length $\sqrt{2}a_{surf}$ that is oriented along either [100] or [010], yield prototypes with prominent (111) facets and may be useful in identifying low-energy reconstructions of the edge along adjoining {111} surfaces.

Although the number of generated reconstruction prototypes increases exponentially with unit-cell area, any characterization information about an observed reconstruction, such as the surface unit-cell lattice vectors, significantly limits the number of prototypes that must be considered in order to determine its structure. Likewise, if STM data are available, a visual comparison between micrographs and structural models is useful to identify the most plausible candidates before performing energy calculations. Also, it is a convenient feature of the zinc-blende (001) surface cell that, if a unique unit cell can be formed under a 90° rotation of lattice vectors, the two unit cells produce the same set of reconstruction prototypes, to within an exchange of species. Thus, nearly half of the possible prototypes can be generated by inspection from the other half.

The excess surface charge was calculated for each generated structure using Eq. (A3). The excess charge histogram, which shows the distribution of excess charge values for the entire set of generated configurations is shown in Fig. 3(b). The distribution is bimodal, with odd-unit-area structures centered at $-1.5e$ and even-unit-area structures centered at charge neutrality.

B. Reconstruction stability of GaAs(001)

We use our database of reconstruction candidates to study GaAs(001) by first identifying the stable and near-stable surface reconstructions in the As-rich regime from first principles. Although GaAs(001) is relatively well studied, until now there has been no comprehensive and systematic method to make theoretical predictions of its phase stability. We apply our approach to the (4×2), (2×4), $c(4\times4)$, $c(8\times2)$, and (4×3) unit cells. The first four are widely reported in the experimental literature to have stable reconstructions.[26,31–33] We consider the (4×3) reconstruction due to the importance of predicting near-stable reconstructions that may manifest in kinetically limited regimes or upon small changes to the material system. A number of experimental results strongly suggest that a (4×3) reconstruction is near-stable or even stable on GaAs(001), including observation of a (4×3) or $(n\times3)$ reconstruction on the pure GaAs surface at low temperature[15] and during reconstruction transitions.[34] Additionally, the occurrence of a (4×3) reconstruction on the chemically similar GaSb(001) is well known,[35] and a $(n\times3)$ reconstruction can be induced on GaAs(001) by submonolayer deposition of InAs.[36] Using our algorithm, we determine there to be 23 (4×2), 23 (2×4), 20 $c(4\times4)$, 20 $c(8\times2)$, and 124 (4×3) reconstruction prototypes that obey the electron counting rule.

Energies of these structures were calculated using DFT as implemented in the VASP code[37] with ultrasoft pseudopotentials.[38] Calculations were performed within the local density approximation (LDA), using the Ceperley-Alder correlation functional[39] as parameterized by Perdew and Zunger.[40] To calculate these energies a slab of six bulk-like atomic bilayers of GaAs was used to approximate the GaAs substrate, terminated above the top layer by the reconstructed surface. The bottom atomic bilayer was fixed at the GaAs lattice parameter of 5.59 Å, as determined by LDA DFT. Atoms in all other layers, and in the reconstructed surface, were allowed to relax to their stable energy minima. We performed calculations at a plane-wave energy cutoff of 350 eV and using a uniform k-point density of 144 k-points

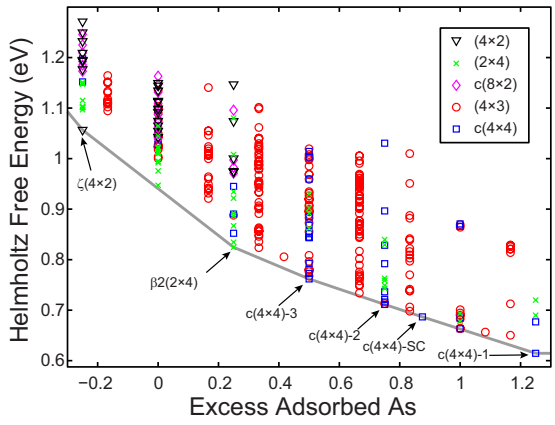

FIG. 4. (Color online) Surface Helmholtz free energies of all 362 calculated reconstructions are shown with respect to excess adsorbed As. 18 configurations lie outside the depicted composition range. Ground states are indicated by arrows and labeled. $c(4\times4)$ variants correspond to configurations depicted in Fig. 2, except for $c(4\times4)$-SC which is a supercell configuration larger than the $c(4\times4)$ unit cell. Data-point markers correspond to unit cell shape, as indicated.

per $(2\pi)^2/a_{surf}^2$ reciprocal area within the plane of the slab; a single k-point was used in the direction normal to the slab. Calculations ranged in size from 90–280 atoms. The slab was separated from its periodic image by approximately 12 Å of vacuum, and each As on the bottom surface was passivated by two pseudohydrogen, having nuclear charge $Z=0.75$, to minimize electrostatic self-interaction across the vacuum layer. The VASP-implemented dipole correction was tested on a range of low-energy reconstructions to determine if dipole interactions across the vacuum layer must be explicitly accounted for but no meaningful difference in energy was observed for the charge-neutral surfaces being considered here.

To analyze reconstruction stability we consider the surface excess Helmholtz free energy, γ, and the surface excess grand potential, which is a Legendre transform of γ given by $\sigma=\gamma-\mu_{\mathrm{As}}x_{\mathrm{As}}^{xs}$, where x_{As}^{xs} is the surface excess adsorbed As; all quantities are normalized by integral unit area. These quantities are defined and their relation to reconstruction stability are described in greater detail in the Appendix B. Both thermodynamic potentials are useful, depending on the boundary conditions of the system. Experimentally μ_{As} is the controlled parameter, fixed by the choice of As vapor pressure and temperature, such that reconstruction stability is determined by minimization of the surface excess grand potential, which is continuous over the range of μ_{As}. For first-principles energy calculations, we must consider specific atomic configurations, each having a fixed composition. To analyze these data we calculate the surface excess Helmholtz free energy, which is the natural thermodynamic potential to use when holding x_{As}^{xs} constant.

Figure 4 depicts the zero-temperature (i.e., without entropic contribution) surface excess Helmholtz free energies versus x_{As}^{xs} for all calculated species configurations of each reconstruction prototype considered. The convex hull of ground-state reconstructions is also shown. In a binary system the convex hull is the curve that describes the lowest possible energy of the system. In Fig. 4 it is the lowest lying convex curve that passes through a subset of data points and connects these ground-state reconstructions by straight "common tangent" lines. A ground state is the equilibrium configuration of the system at a given composition; at compositions between two ground states the system exhibits phase separation between the two proximal ground states with a Helmholtz free energy on their common tangent line. The convex hull provides a clear reference to determine how close a reconstruction is to stability, which is measured as the difference in energy between the reconstruction and the convex hull. We focus on those reconstruction prototypes within less than 50 meV of the convex hull, of which there are nine. Structural diagrams of these prototypes are shown in Fig. 5.

The potential to limit the field of 210 reconstruction prototypes to the nine most likely candidates near the convex hull demonstrates the importance of an objective measure of relative stability that is compatible with the computational process. Having limited our consideration to only nine reconstruction prototypes it is reasonable to begin calculating first principles energies of species configurations for each prototype by substituting Ga for As (or visa versa when possible) at threefold coordinated sites. The database of these calculations can be used to construct and refine a cluster expansion for each reconstruction prototype that describes the energetics of Ga-As disorder over the threefold coordinated sites.

We explored the range of species configuration on the threefold coordinated sites of the low-energy $h0(4\times3)$ and $c(4\times4)$ prototypes from Fig. 5, focusing on the sites indicated in Fig. 2. Each site belongs to a surface dimer and, because it has three-fold coordination, can undergo Ga-As substitution. Initial calculations demonstrated that the sites on the $h0(4\times3)$ trench dimer [circled in Fig. 2(a)] exhibit a large energy increase upon exchanging As for Ga. Since thermal excitations of occupancy at these sites would be relatively rare events at moderate temperatures in the As-rich regime, they were excluded from further analysis. The remaining threefold coordinated sites of the $h0(4\times3)$ and $c(4\times4)$ prototypes (indicated in Fig. 2) were considered in constructing the cluster expansion for each prototype. The cluster expansion for the $h0(4\times3)$ prototype was constructed from a set of 49 configurational energies to parameterize six site, 11 pair, and three triplet ECI with a cross-validation score of 1.8 meV per considered dimer site of the unit cell. The cluster expansion for the $c(4\times4)$ prototype was constructed from a set of 17 configurational energies to parameterize two site, five pair, and two triplet ECI with a cross-validation score of 0.7 meV per dimer site. Like the atomic sites of the $h0(4\times3)$ trench dimer, the dimer sites of the $\beta(2\times4)$ have high As-Ga substitution energies. Since the most stable species configuration identified for the $\beta(2\times4)$ prototype is also the most As rich, we did not construct a $\beta(2\times4)$ cluster expansion.

Using the two cluster expansions to perform a convex hull analysis, we identified ten low-energy site configurations of the $h0(4\times3)$ prototype and five low-energy site configurations of the $c(4\times4)$ prototype. The predicted energies of these site configurations were confirmed by DFT calculations and no configurations with lower energies were predicted by the cluster expansions. Figure 2 shows depictions of the

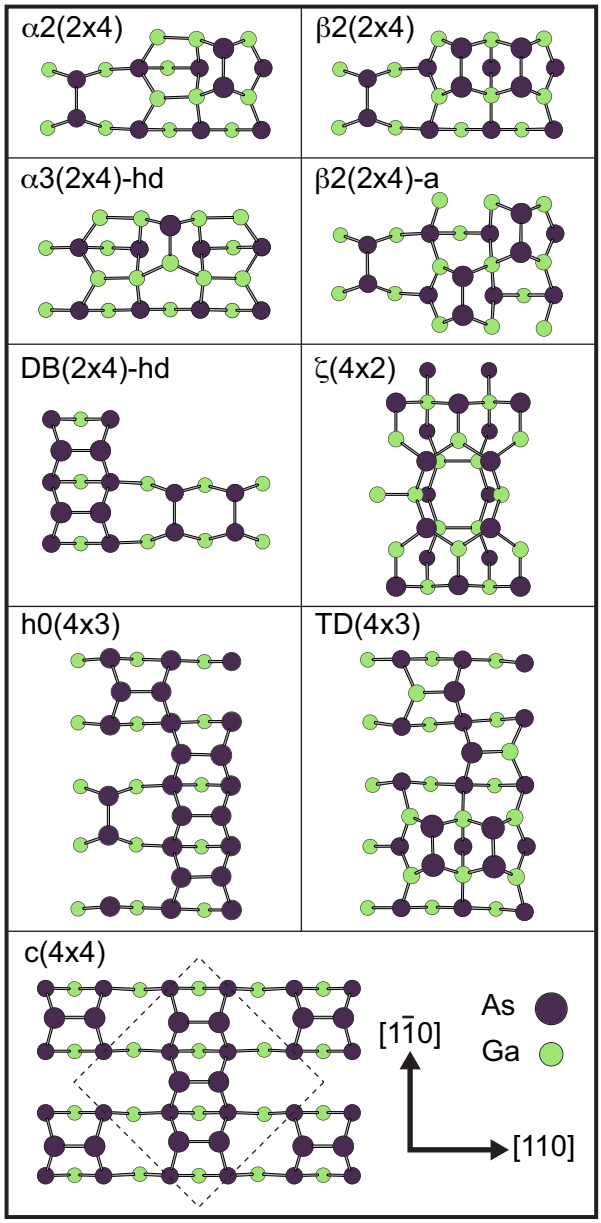

FIG. 5. (Color online) Structural models of stable and near-stable reconstructions of GaAs (001), as determined by our calculations.

identified low-energy configurations that can be described within the prototype unit cells. Of the low-energy configurations found, four $c(4\times4)$ site configurations are reconstruction ground states of the GaAs(001) surface. The lowest energy configuration of the $h0(4\times3)$ comes within about 2 meV per integral unit area of being stable and six of its ten low-energy species configurations are within 10 meV of the total convex hull. In addition to the four $c(4\times4)$ reconstruction ground states, the total convex hull of GaAs(001) reconstructions includes the $\beta2(2\times4)$ at slightly lower x_{As}^{xs} and the highly Ga-enriched $\zeta(4\times2)$ reconstruction, the latter of which was not generated by our algorithm but was included as a Ga-rich limiting case.

To study the intermediate-temperature thermodynamics of the $h0(4\times3)$ and $c(4\times4)$ prototypes, we applied Monte

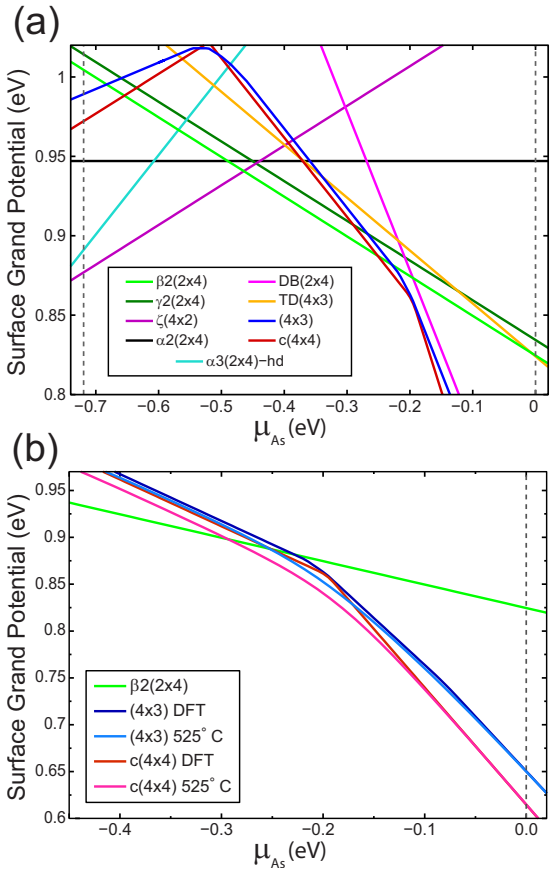

FIG. 6. (Color online) (a) Surface excess grand potential energies of GaAs(001) reconstructions within 20 meV of the convex hull, calculated from DFT. For simplicity and consistency, dimer-site configurations of the $h0(4\times3)$ and $c(4\times4)$ prototypes are each shown as a single line. (b) Surface excess grand potential of the $c(4\times4)$ and $h0(4\times3)$ prototypes and the $\beta2(2\times4)$ reconstruction in the As-rich regime. Finite temperature surface grand potentials of $c(4\times4)$ and $h0(4\times3)$ are also shown, calculated with Monte Carlo at 525 °C using the optimized cluster expansions. Dashed lines indicate the chemical potential at which the surface becomes unstable relative to bulk As (on the right) and bulk Ga (on the left).

Carlo simulation techniques to the optimized cluster expansion of each reconstruction within the semigrand canonical ensemble. The surface excess grand potential can then be obtained via integration.[14] Figure 6(b) shows the surface excess grand potential, σ, for the $h0(4\times3)$ and $c(4\times4)$ prototypes at 525 °C in the As-rich regime with 0 K DFT results shown for comparison. The $c(4\times4)$ becomes significantly more stable relative to the $h0(4\times3)$ as temperature is increased. Additionally, the dimer sites of the two prototypes exhibit a solid solution behavior, where there are no ordering phase transitions at physically relevant temperatures. Trends in the relative stability are illustrated more clearly in Fig. 7, which shows $\Delta\sigma=\sigma_{h0(4\times3)}-\sigma_{c(4\times4)}$ in the As-rich regime. We compare 0 K results for the $\beta2(2\times4)$ to the finite-temperature results to approximate the chemical potential range over which the $c(4\times4)$ prototype is stable at finite temperature. This is not an unreasonable approximation, since the $\beta2(2\times4)$ cannot become more As-rich without forming antisite defects. Thus, at finite temperatures its sta-

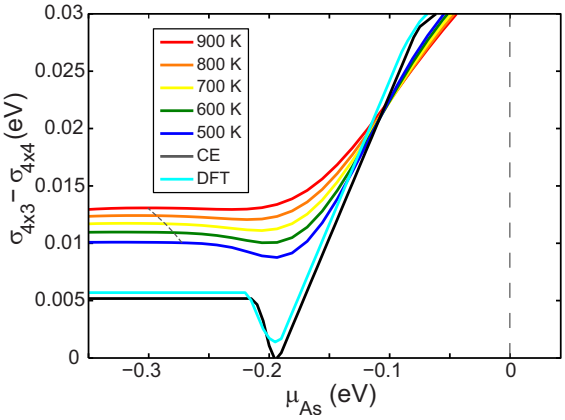

FIG. 7. (Color online) The difference in surface grand potential energies of the $h0(4\times3)$ and $c(4\times4)$ prototypes are plotted with respect to As chemical potential. Differences are shown at several temperatures, calculated from Monte Carlo using the optimized cluster expansions. 0 K results are shown comparing cluster expansion predictions to DFT energy calculations.

bility will not encroach significantly upon that of the As-rich $c(4\times4)$.

IV. DISCUSSION

A database of the likely reconstruction prototypes of the III-V (001) surface systems will significantly expedite the future study of these material systems. Especially as the focus of study within III-V surface science continues to expand into systems with larger numbers of alloying components and wider ranges of alloy compositions, a trial and error approach to constructing reconstruction prototypes is insufficient to characterize these complex surfaces, and the likelihood for redundancy of effort is high. Having a database of prototypes will enable automated characterization using real-space and reciprocal-space experimental data along with predictive-adaptive models of electronic structure effects. Additionally, the possibility of exploring structural and configurational degrees of freedom in an efficient and systematic way in order to exhaustively identify likely reconstruction prototypes demonstrates the significant opportunity that exists for constructing similar databases for many other material systems.

For the generated III-V (001) prototypes, a surprising distinction between two basic classes of generated arises from Eq. (A3) that determines the ability of a reconstruction to satisfy the electron counting model. It is clear that the excess bilayer charge in Eq. (A3) must always take an integer value. By contrast, the excess charge donated by the bulk is $\frac{3}{2}N_A$, where N_A is the integral unit area defined by Eq. (2); this contribution has an integer value for even unit area but has a half-integer value for odd unit area. This implies that a III-V (001) surface reconstruction with odd unit area can never obey the electron counting model if it follows the basic structural rules we have outlined and has no fourfold coordinated antisites. This unexpected result may account for the lack of any verified (001) III-V surface reconstructions with odd unit area. Although references to (1×3) and (1×5) reconstructions can be found in the literature, structural models for these reconstructions that are verifiable from first principles are lacking. Experimental characterization techniques that lead to such nomenclature use reciprocal space measurements, which can be significantly affected by thermal excitations of the surface. Thermal disorder along one or both axes can cause phase decoherence at smaller Bragg angles, shortening apparent lattice periodicities by a factor of two or more of the actual periodicity that exists at short length scales, where the ECM may be satisfied.

After considering all (4×3) reconstruction prototypes that obey the anion-rich structural guidelines, we have found that the $h0(4\times3)$ reconstruction prototype, which was originally proposed by Barvosa-Carter, *et al.*[35] to explain observations on GaSb and AlSb, is very nearly stable on pure GaAs(001). We have determined that the $h0(4\times3)$ structural model is the only candidate that is near the convex hull. As such, it is by far the most likely candidate prototype for the (4×3) reconstruction that is observed in some regimes on $In_xGa_{1-x}As(001)$ and the InAs wetting layer on GaAs(001). It is important to note that the energy differences are within the error range expected from DFT approximations and implementation. As such, the $h0(4\times3)$ prototype is sufficiently close to the convex hull that previously reported experimental observations of a (4×3) or $(n\times3)$ reconstruction on pure GaAs (Refs. 15 and 34) indicate that dimer-site configurations of the $h0(4\times3)$ prototype may actually be stable at equilibrium over a small region of temperature and chemical potential. Also, differences in vibrational free energy between prototypes, which have not been considered here, are another possible stabilization mechanism. Even if it is not stable, observations of the (4×3) reconstruction on pure GaAs may be due to sample preparation along a thermodynamic path that limits growth kinetics, resulting in a metastable $h0(4\times3)$ surface.

Although the finite-temperature behavior of the $c(4\times4)$ has been investigated previously,[41] the physical model used was not predictive and did not explore the entire configurational phase space and thus would be unsuitable for comparing the stability of two different reconstructions at finite temperature. Additionally, the very small energy difference between $h0(4\times3)$ and $c(4\times4)$ prototypes was apparently not realized at the time, and no comparison was made between the two prototypes. Our method identifies the same $c(4\times4)$ ground states predicted by the trial-and-error enumerative method employed in that work, as well as a $N_A=16$ supercell that is a ground-state configuration containing four Ga-As heterodimers.

In addition to the two reconstructions on which we have focused most intently, our methods have yielded a number of other low-energy reconstructions that are less than 50 meV from the convex hull (with surface excess grand potentials plotted in Fig. 6). These represent structures which might occur as metastable phases, along surface phase domain boundaries, or as isolated defects of more stable reconstructions. Alternatively, they might occur as intermediate structures during layer-by-layer growth. Structural illustrations of these reconstructions, as well as the ground states, are shown in Fig. 5.

The nonground-state structures that are shown are the cation-rich $\alpha3(2\times4)$ with heterodimer termination;[42] the

$\beta 2(2\times 4)-a$, which is an alternate dimerization of the $\beta 2(2\times 4)$ and may occur as a low-energy defect; the $\alpha 2(2\times 4)$, which is well-known as a ground-state reconstruction of InAs(001); the $DB(2\times 4)$, which has a prominent dimer backbone; and the $TD(4\times 3)$, which is similar in structure to the $h0(4\times 3)$ but taller, with a prominent double dimer feature. A careful survey of the literature shows that most of these structures have been considered previously, either as dilute defects or as equilibrium reconstructions of other materials systems. However, in the case of the $DB(2\times 4)$ (Ref. 35) or the $TD(4\times 3)$,[16] the structures were proposed only to explain local defects of $\times 3$ reconstructions in STM micrographs; no names or first-principles energy analyses could be found for these reconstructions.

In the Ga-rich regime of the GaAs(001) surface we confirmed that the $\zeta(4\times 2)$ reconstruction is stable. This result is consistent with published results for the Ga-rich GaAs(001) surface.[43] The $\zeta(4\times 2)$ is the only well-accepted reconstruction ground state that violates the rules we have enumerated due to the sp^2 bond character of its Ga-Ga bonds. It should be noted that the $\zeta(4\times 2)$ was originally derived from a previously proposed structure, the $\beta(4\times 2)$, which does obey our structural rules. The related $\zeta(4\times 2)$ structure can be obtained by perturbing a six-atom structural motif of the $\beta(4\times 2)$ by $a/4$ along the [110] direction and then using DFT energy minimization to relax the ion positions.[43]

At the group III-rich extreme, the necessary group III-group III bonds result in under filling of some $\sigma(sp^3)$ orbitals, leading to a combination of $\sigma(sp^3)$ and $\sigma(sp^2)$ bonding orbitals to be energetically preferred. The resultant sp^2 character of the surface group-III bonds manifests in more trigonal bond angles, giving rise to fundamentally different surface motifs, such as those seen in the $\zeta(4\times 2)$. Although our method could be applied to these bonding environments, for now we have chosen to focus on the group-V-rich regime, where more application-driven interest is focused. Considering that the $\zeta(4\times 2)$ can be constructed by perturbing and relaxing the atom positions of the $\beta(4\times 2)$, we suggest that a possible approach to exploring the group-III-rich regime would be to attempt various translational perturbations of promising structural candidates that obey our proposed structural rules. Specific perturbations should be chosen in an attempt to free the structures from shallow minima of the potential energy surface and promote trigonal bonding of locally group-III-enriched features. Physically motivated guidelines similar to those we have laid out for the group-V-rich regime could be used to identify structures most likely to benefit from perturbation toward trigonal-type bonding and to identify appropriate perturbations based on the symmetry of the reconstruction prototype.

V. CONCLUSION

We have presented a comprehensive and tractable approach to resolving gaps in understanding of surface reconstruction phase diagrams where an experimentally observed but poorly characterized reconstruction phase exists or even in lieu of such evidence. This approach was demonstrated by conducting a study of the zinc-blende III-V (001) surface in the group-V-rich regime, for which we have codified the structural rules obeyed by observed structural motifs. A comprehensive database of likely reconstructions was efficiently constructed using our algorithm, providing a valuable resource for analyzing surface phenomena of these systems and for predicting new equilibrium reconstructions for poorly understood systems.

Our in-depth study of the GaAs(001) surface using this database of reconstruction prototypes represents the most comprehensive analysis of GaAs(001) reconstruction stability to date, not only by taking into consideration all likely reconstruction prototypes, but also by rigorously including the effects of configurational disorder of homo/heterodimer site occupancy at finite temperature. From this analysis we have demonstrated that the $h0(4\times 3)$ reconstruction prototype is much more energetically competitive with the $c(4\times 4)$ than previously thought. Moreover, because our analysis included all charge-neutral (4×3) reconstruction prototypes that are likely, given our understanding of the III-V (001) surface, we have demonstrated that the $h0(4\times 3)$ reconstruction prototype is the most likely candidate for the (4×3) reconstruction observed on $In_xGa_{1-x}As$ (001) and at low temperature on GaAs(001).

ACKNOWLEDGMENTS

We gratefully acknowledge support from DOE/BES (ER 46172). This work was performed in part at the U.S. Department of Energy, Center for Integrated Nanotechnologies, at Los Alamos National Laboratory (Contract No. DE-AC52-06NA25396) and Sandia National Laboratories (Contract No. DE-AC04-94AL85000).

APPENDIX A: SIMPLIFIED ELECTRON COUNTING MODEL FOR GENERATED PROTOTYPES

Starting from the first three structural rules enumerated in Sec. II A, we can construct an expression for the electron counting rule that is general for all candidate structures generated by our algorithm (as well as those with "bridged" motifs and linear polymers, which are not generated). To do this we examine a single atomic bilayer, consisting of anion monolayer i, which is nearer to the bulk, and cation monolayer $i+1$, which is nearer to the surface. In that case the excess number of electrons in the bilayer j that contains monolayers i and $i+1$ is

$$(\Delta q)_j = 2(B_i + B_{i+1}) - 5N_{i+1} - 3N_i, \tag{A1}$$

where B_i is the total number of bulk-oriented bonds, in-plane bonds, and *filled* dangling bonds belonging to layer i, and N_i is the number of atoms in layer i. This is a simple charge-balance equation with coefficients arising from the five valence electrons of the anion species and three valence electrons of the cation species and the requirement that filled orbitals contain two electrons. We assume for now that there are no antisites.

From the first three structural rules, the bonding term in Eq. (A1) can be expressed as

$$B_i + B_{i+1} = [2(N_i + N_{i+1}) + D_i + D_{i+1}] + [2(N_i - N_{i+1}) - 2D_i]. \tag{A2}$$

The left bracketed term accounts for all bulk-oriented bonds (of which each atom has two) and in-plane bonds formed by atoms in the bilayer, where D_i denotes the number of in-plane bonds between atoms in layer i. The right bracketed term accounts for all dangling bonds in the anion layer. This can be seen by noting that, absent any in-plane bonds, if layer $i+1$ has one atom fewer than layer i, two dangling bonds must exist in layer i. In general, the number of filled dangling bonds created in layer i is twice the difference between the number of anions in layer i and the number cations in layer $i+1$ due to the constraint of structural rule 3. Since layer i consists of anions, these dangling bonds must be filled. We then must twice the number of dangling bonds in layer i since each anion in-plane bond destroys two anion dangling bonds.

By substituting Eq. (A2) into Eq. (A1) we obtain

$$(\Delta q)_j = 3(N_{i+1} - N_i) + 2(D_i - D_{i+1}). \tag{A3}$$

This expression can be used to find the total number of excess electrons by summing over all bilayers of the structure, assuming that the first bulklike layer of cations contributes $\frac{3}{2}N_A$ electrons to the surface, where N_A is defined in Eq. (2). This is a very simple form of the ECM, and with our convention of abstracting the dimer bond as a distinct specie, excess charges are determined for a database of thousands of candidate structures in a matter of seconds.

APPENDIX B: THERMODYNAMIC DESCRIPTION OF MULTICOMPONENT SURFACES

The surface excess Helmholtz free energy of a semi-infinite with a planar surface can be considered as the difference in the Helmholtz free energy of a sufficiently thick region of the slab that encloses the surface and that of an equivalent quantity of bulk material. Although this is straightforward for elemental materials, it is complicated for multicomponent systems by the possibility that the surface composition is different from the range of allowed bulk compositions. Thus, we write the surface excess Helmholtz free energy as

$$\gamma = (E_{slab} - N_{\mathrm{Ga}}E^{bulk}_{\mathrm{GaAs}} - N_{\mathrm{As}}E^{bulk}_{\mathrm{As}})/N_A - E_T, \tag{B1}$$

where E_{slab} is the first-principles energy of the slab geometry described in Sec. III B and E_T is a correction accounting for the pseudohydrogen termination of the bottom surface. In Eq. (B1) we have subtracted the energy of a two-phase As/GaAs bulk coexistence, where the number of Ga are taken to be the number of GaAs formula units. We can select arbitrary reference states when expressing γ, but we choose reference states in Eq. (B1) such that the surface excess Ga is always zero and the reference As chemical potential corresponds to metallic As.

The area normalized γ of Eq. (B1) can be used to compare the stability of different reconstructions using a convex hull construction along the composition variable x^{xs}_{As}, which is defined

$$x^{xs}_{\mathrm{As}} \equiv (N_{\mathrm{As}} - N_{\mathrm{Ga}})/N_A. \tag{B2}$$

We may consider γ with respect to only one composition, despite describing an open system, since this particular description essentially decomposes energy differences into those due to the addition of bulklike material (which is trivial) and those due to changes in stoichiometry at the surface.

*avdv@umich.edu

[1] P. Kratzer, E. Penev, and M. Scheffler, Appl. Surf. Sci. **216**, 436 (2003).
[2] G. A. Somorjai, Annu. Rev. Phys. Chem. **45**, 721 (1994).
[3] G. Zhou and J. Yang, J. Mater. Res. **20**, 1684 (2005).
[4] U. Welp, V. K. Vlasko-Vlasov, X. Liu, J. K. Furdyna, and T. Wojtowicz, Phys. Rev. Lett. **90**, 167206 (2003).
[5] J. Houze, S. Kim, S.-G. Kim, S. C. Erwin, and L. J. Whitman, Phys. Rev. B **76**, 205303 (2007).
[6] J. Schnadt, J. Knudsen, X. L. Hu, A. Michaelides, R. T. Vang, K. Reuter, Z. Li, E. Lægsgaard, M. Scheffler, and F. Besenbacher, Phys. Rev. B **80**, 075424 (2009).
[7] J. M. Millunchick, A. Riposan, B. J. Dall, C. Pearson, and B. G. Orr, Surf. Sci. **550**, 1 (2004).
[8] C. W. Glass, A. R. Oganov, and N. Hansen, Comput. Phys. Commun. **175**, 713 (2006).
[9] S. Curtarolo, D. Morgan, K. Persson, J. Rodgers, and G. Ceder, Phys. Rev. Lett. **91**, 135503 (2003).
[10] C. C. Fischer, K. J. Tibbetts, D. Morgan, and G. Ceder, Nature Mater. **5**, 641 (2006).
[11] F. Chuang, C. Ciobanu, V. Shenoy, C. Wang, and K. Ho, Surf. Sci. **573**, L375 (2004).
[12] J. M. Sanchez, F. Ducastelle, and D. Gratias, Physica A **128**, 334 (1984).
[13] D. De Fontaine, in *Solid State Physics*, edited by H. Ehrenreich and D. Trunbull (Academic, New York, 1994), p. 33.
[14] J. C. Thomas, J. M. Millunchick, N. A. Modine, and A. Van der Ven, Phys. Rev. B **80**, 125315 (2009).
[15] L. Däweritz and R. Hey, Surf. Sci. **236**, 15 (1990).
[16] Y. Garreau, K. Aïd, M. Sauvage-Simkin, R. Pinchaux, C. F. McConville, T. S. Jones, J. L. Sudijono, and E. S. Tok, Phys. Rev. B **58**, 16177 (1998).
[17] L. E. Sears, J. M. Millunchick, and C. Pearson, J. Vac. Sci. Technol. B **26**, 1948 (2008).
[18] M. D. Pashley, Phys. Rev. B **40**, 10481 (1989).
[19] J. Neugebauer, T. Zywietz, M. Scheffler, J. E. Northrup, and C. G. Van de Walle, Phys. Rev. Lett. **80**, 3097 (1998).
[20] H. A. H. AL-Brithen, R. Yang, M. B. Haider, C. Constantin, E. Lu, N. Sandler, A. R. Smith, and P. Ordejón, Phys. Rev. Lett. **95**, 146102 (2005).

[21] W. A. Harrison, *Electronic Structure and the Properties of Solids: The Physics of the Chemical Bond* (Freeman, San Francisco, 1980).
[22] L. J. Whitman, P. M. Thibado, S. C. Erwin, B. R. Bennett, and B. V. Shanabrook, Phys. Rev. Lett. **79**, 693 (1997).
[23] P. Laukkanen, M. P. J. Punkkinen, H.-P. Komsa, M. Ahola-Tuomi, K. Kokko, M. Kuzmin, J. Adell, J. Sadowski, R. E. Perälä, M. Ropo, T. T. Rantala, I. J. Väyrynen, M. Pessa, L. Vitos, J. Kollár, S. Mirbt, and B. Johansson, Phys. Rev. Lett. **100**, 086101 (2008).
[24] L. Ferreira, S.-H. Wei, and A. Zunger, Int. J. High Perform. Comput. Appl **5**, 34 (1991).
[25] G. L. W. Hart and R. W. Forcade, Phys. Rev. B **80**, 014120 (2009).
[26] T. Arai, M. Suzuki, Y. Ueno, J. Okabayashi, and J. Yoshino, Proceedings of the 14th International Conference on Molecular Beam Epitaxy, 2006; [J. Cryst. Growth **301-302**, 22 (2007)].
[27] A. Van der Ven, J. C. Thomas, Q. Xu, B. Swoboda, and D. Morgan, Phys. Rev. B **78**, 104306 (2008).
[28] A. van de Walle and G. Ceder, J. Phase Equilib. **23**, 348 (2002).
[29] B. C. Han, A. Van der Ven, G. Ceder, and B.-J. Hwang, Phys. Rev. B **72**, 205409 (2005).
[30] G. Hart, V. Blum, M. Walorski, and A. Zunger, Nature Mater. **4**, 391 (2005).
[31] Q. Xue, T. Hashizume, J. M. Zhou, T. Sakata, T. Ohno, and T. Sakurai, Phys. Rev. Lett. **74**, 3177 (1995).
[32] M. D. Pashley, K. W. Haberern, W. Friday, J. M. Woodall, and P. D. Kirchner, Phys. Rev. Lett. **60**, 2176 (1988).
[33] H. Xu, Y. Y. Sun, Y. G. Li, Y. P. Feng, A. T. S. Wee, and A. C. H. Huan, Phys. Rev. B **70**, 081313 (2004).
[34] I. Chizhov, G. Lee, R. F. Willis, D. Lubyshev, and D. L. Miller, Phys. Rev. B **56**, 1013 (1997).
[35] W. Barvosa-Carter, A. S. Bracker, J. C. Culbertson, B. Z. Nosho, B. V. Shanabrook, L. J. Whitman, H. Kim, N. A. Modine, and E. Kaxiras, Phys. Rev. Lett. **84**, 4649 (2000).
[36] T. J. Krzyzewski, P. B. Joyce, G. R. Bell, and T. S. Jones, Surf. Sci. **517**, 8 (2002).
[37] G. Kresse and J. Furthmüller, Phys. Rev. B **54**, 11169 (1996).
[38] D. Vanderbilt, Phys. Rev. B **41**, 7892 (1990).
[39] D. M. Ceperley and B. J. Alder, Phys. Rev. Lett. **45**, 566 (1980).
[40] J. P. Perdew and A. Zunger, Phys. Rev. B **23**, 5048 (1981).
[41] E. Penev, P. Kratzer, and M. Scheffler, Phys. Rev. Lett. **93**, 146102 (2004).
[42] W. Schmidt, Appl. Phys. A: Mater. Sci. Process. **75**, 89 (2002).
[43] S.-H. Lee, W. Moritz, and M. Scheffler, Phys. Rev. Lett. **85**, 3890 (2000).